

Article

Numerical Multifield Coupling Model of Stress Evolution and Gas Migration: Application of Disaster Prediction and Mining Sustainability Development

Xiangguo Kong^{1,2}, Tianshuo Zhao^{1,2,*}, Yuchu Cai^{1,3} and Di He^{1,3}

¹ College of Safety Science and Engineering, Xi'an University of Science and Technology, Xi'an 710054, China; kxgtudou7218@xust.edu.cn (X.K.); caiyuchu@126.com (Y.C.); hd0089001@163.com (D.H.)

² Key Laboratory of Western Mine and Hazard Prevention, Ministry of Education of China, Xi'an 710054, China

³ School of Chemistry and Chemical Engineering, Xi'an University of Science and Technology, Xi'an 710054, China

* Correspondence: 22220226178@stu.xust.edu.cn

Abstract: At present, coal mining is gradually shifting towards deep areas, and coal mines under deep mining conditions are more prone to coal and gas outburst accidents. In this research, we aim to explain the causes and mechanisms of dynamic disasters, which are caused by the combined action of static load, gas, and dynamic load on tectonic regions in complex stress field environments. Through numerical simulation using COMSOL Multiphysics software, based on the geological conditions of a mine in Jilin Province, it was found that faults lead to abnormal stress in tectonic regions. The combined action of dynamic and static loads results in excessive stress, causing the fragmentation and displacement of the coal body, leading to coal mine disasters, thus disrupting sustainability. Additionally, the coal matrix gas entering fractures raises the gas pressure and leads to the accumulation of methane near earthquake sources. Dynamic loads accelerate gas desorption in coal and increase porosity and permeability, facilitating rapid gas migration. This influx of gas into the roadways exceeds safety limits. Then, based on these findings and on-site conditions, a set of sustainable measures for coal mines has been proposed. This research offers theoretical guidance for enhancing safety, stability, and sustainability in coal mining processes.



Citation: Kong, X.; Zhao, T.; Cai, Y.; He, D. Numerical Multifield Coupling Model of Stress Evolution and Gas Migration: Application of Disaster Prediction and Mining Sustainability Development. *Sustainability* **2024**, *16*, 3667. <https://doi.org/10.3390/su16093667>

Academic Editor: Cun Zhang

Received: 12 March 2024

Revised: 23 April 2024

Accepted: 23 April 2024

Published: 27 April 2024



Copyright: © 2024 by the authors. Licensee MDPI, Basel, Switzerland. This article is an open access article distributed under the terms and conditions of the Creative Commons Attribution (CC BY) license (<https://creativecommons.org/licenses/by/4.0/>).

Keywords: dynamic disaster; sustainability; stress; porosity; permeability; numerical simulation

1. Introduction

In recent decades, the coal mining depth in China has been increasing [1–3]. Nowadays, the mining depth in some mines has exceeded one kilometer, and it is increasing at a rate of more than ten meters every year [4,5]. The in situ stress, gas pressure and gas content increase with the increase in mining depth [6,7], and the stope structure is becoming more and more complex [8–10]. The frequency, intensity and damage degree of rock burst disasters are on the rise, so the number of accidents caused by coal and gas outbursts are also increasing; the sustainable development of coal mining production faces significant challenges [11,12]. Therefore, revealing the stress evolution and gas migration laws during the dynamic disaster process in coal mines and specifying targeted measures are of great significance for improving the safety and sustainability of coal mines.

Considering the actual coupling conditions of the coal body, a study of the multifield coupling mechanisms of gas-bearing coal has great guiding significance for disaster prevention and control. Currently, many scholars are conducting extensive research in this field. Yu et al. (2024) innovatively explored the qualitative and quantitative effect of axial stress loads on the low-temperature oxidation behaviors of loose broken coal using a multifield coupled numerical simulation [13]. Zhao et al. (2020) established a multifield coupling model based on the heterogeneity of coal seams, and numerically simulated the

mining process of horizontal and fault coal seams. Then, they analyzed the evolution of gas pressure and magnetic permeability under different parameters [14]. Yang et al. (2011) built an air–solid coupling model for the fracture process of gas-bearing coal/rock, which was based on the coupling effects of stress, damage, and permeability evolution during coal deformation [15]. Wang et al. (2012) combined the dynamic model of porosity and permeability with the stress and seepage equations of gas-bearing coal, and established an air-structure coupling model of gas-bearing coal [16]. Liu et al. (2017) proposed a permeability model based on dynamic diffusion, evaluated the sensitivity of the model to the parameters, and discussed the determination of permeability rebound and effective drilling radius. [17]. Xue et al. (2011) finished a three-dimensional solid–liquid–gas coupling numerical analysis of coal and gas outburst, and found coal seam mining and geological sedimentary conditions were the main factors affecting the risk of outbursts [18]. Wang et al. (2023) constructed a multifield gas desorption diffusion model coupled with mechanical field, thermal field, and gas diffusion field, considering the parallel and series structures between macropores and micropores, and then solved the gas diffusion process under different structures [19].

The multifield coupling effect of gas-bearing coal was not only limited to laboratory experiments and the construction of theoretical models. Many scholars have established corresponding models based on field practice, and solved the corresponding results numerically to ensure consistency with the real situation on site. Gao et al. (2016), by combining numerical simulation with the “10–20” large-scale coal and gas outburst disaster in the Daping coal mine, believed that stress concentration and mining disturbance in gas enrichment areas were major reasons for coal and gas outbursts [20]. Li et al. (2017) used FLAC 3D to establish a three-dimensional numerical calculation model of cross-cut coal uncovering. Based on the pressure and displacement evolution characteristics of coal mining under different stress angles, the outburst prevention and stability measures of cross-cut coal uncovering were proposed [21]. Zhao et al. (2022) constructed a Multiphysics numerical analysis model for the entire sudden process based on the coupling law of sudden gas heating and fluid structure. They discussed the stress, pressure, temperature, and seepage response laws of different regions and time nodes around the coal rock mass around gas bursts under high stress conditions [22]. Hu et al. (2015, 2016a, 2016b) analyzed the gas release mechanism of coal particles of different scales, established a control equation group and numerical solution for the damage and deformation of gas-bearing coal, and applied it to the coal mine for protective layers mining; the numerical solution results were consistent with the actual situation [23–25]. Liu et al. (2021) integrated the coupling effects of water vapor flow, elastic deformation, and damage, then established a time-varying rock fluid geomechanics model to analyze and model the interaction between the elastic deformation field, the transient fluid transport field, and the discontinuous damage field [26]. Liu et al. (2023) established a coupled multifield model of the stress–strain, gas transport, and damage fields to study the evolution of stress, pressure, and the plastic failure zone under different gradient and coal thickness amplitudes. It was found that changes in coal thickness led to higher stress, higher pressure, and lower coal strength, making it easier to trigger eruptions [27]. Shao et al. (2022) established a stress seepage damage coupling model based on micromechanics, combining the continuous damage model with the effective stress principle to simulate the initiation and propagation of cracks in rock materials and their interaction with fluid flow. [28]. Shu et al. (2022) established three coupled models for the static load, stress disturbance, and dynamic load conditions of the stress and pressure distribution of the coal body in front of the working face. Then, they studied the gas pressure distribution and explosion mechanism, and proved that the high concentration of gas pressure in the coal body in front of the working face is caused by dynamic loads [29]. Zhou et al. (2014) analyzed the propagation characteristics of shock waves and airflow induced by explosive intensity, proposed control equations for shock wave and airflow propagation, and simulated the propagation characteristics of shock wave and airflow coupling using Fluent software [30].

To sum up, the study of the fluid–structure interaction regarding coal and gas has always been a hot spot in mining research, and fruitful results have been achieved so far. However, behind the coal and gas outburst disasters, there are often dynamic changes between stress and gas. In current research, there is still relatively little research on stress evolution and gas migration under multifield coupling in coal and gas outburst accidents. To analyze the mechanism of coal and gas accidents, and to propose targeted sustainable development measures, a numerical model was established using the 5.1 version COMSOL Multiphysics simulation software under the geological conditions of accidents. The stress distribution in the mining space was analyzed, especially the concentrated stress in the tectonic area, and stress evolution within coal mining was also discussed. Then, the stress redistribution, coal deformation and gas migration caused by dynamic load were researched. Finally, by comparing and analyzing the numerical simulations and phenomena, a set of disaster prevention measures that can improve the sustainability and safety of mine development was proposed. These results not only have a promotional effect on the study of the development laws of dynamic disasters, such as coal and gas outbursts during underground mining, but also promote the sustainable development of coal production.

2. Mine Background

The numerical simulation case is based on the coal mine in Jilin Province, China. The mine adopts a multi-level zoning development method. The entire mine is divided into four levels, the first level is above +550 m, the second level is between +400 m and +550 m, the third level is between +206 m and +400 m, and the fourth level is between +100 m and +206 m. The long wall comprehensive mechanized mining method is used in the mine, and the natural cross fall method is used to manage the roof. The excavation face uses blasting excavation. At present, the production level is at the fourth level, with a total of one fully mechanized mining face and four coal roadway excavation faces arranged throughout the mine.

There are four coal seams in this coal mine, which are numbered as layers I~VI. Among them, coal layers I and II are widely developed and are the main coal seams in the coal mine. The remaining coal seams are not mineable except for the local mineable layer III. Coal layer I is a complex coal seam, with a thickness of 0.02~6.3 m. The coal quality is hard, and there is dispersed pyrite. The coal seam contains 1~3 layers of stone, the thickness of a single layer of stone is 0.5~1.0 m. Coal layer II is also a complex coal seam, with a thickness of 0.1~7.9 m, and the coal type is half bright.

The accident case in this paper occurred in coal layer I. In this accident, there were 12 deaths and 1 injury and it was regarded as a major coal and gas outburst. The outburst accident area is shown in Figure 1. From the geological conditions, the excavation tunnel in the accident was surrounded by an igneous rock wall and faults such as a1, a14 and R4. This also indicated that there was tectonic stress in this area.

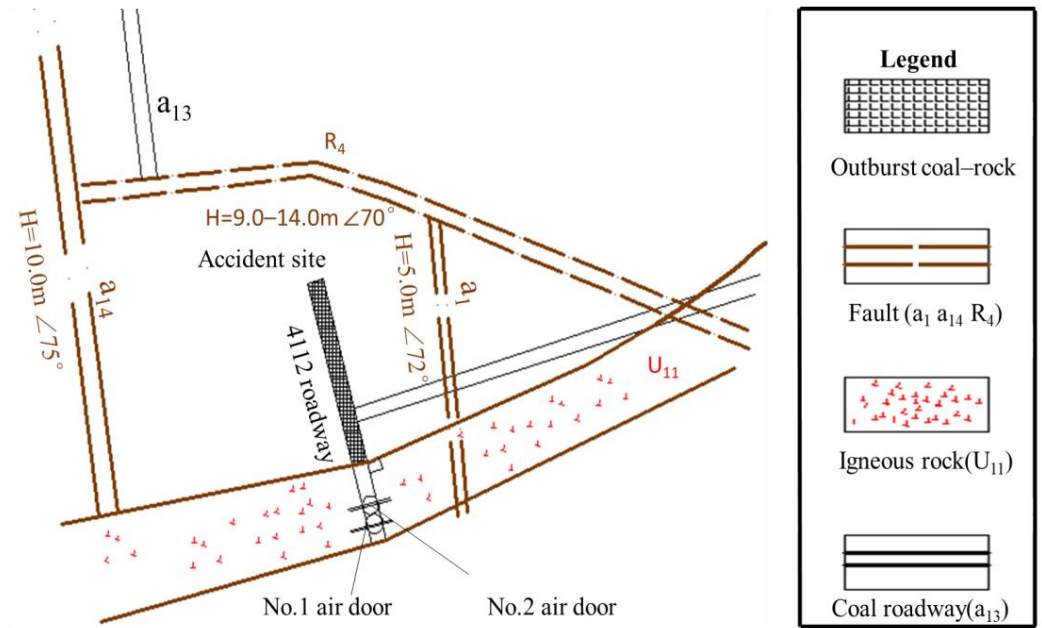


Figure 1. Accident area in numerical simulation case.

3. Numerical Simulation of Disaster Case

3.1. Basic Model and Assumptions

According to the gas-bearing coal impact-dynamics model and the gas migration model under dynamic load, the gas-bearing coal impact-dynamics constitutive equation and gas-bearing coal desorption, diffusion, seepage, and emission equations were established.

(1) Impact-dynamics constitutive equation of gas-bearing coal

Due to comprehensively taking into account factors such as axial static load, confining pressure, gas pressure, and dynamic load, the impact-dynamics constitutive equation of gas-bearing coal was established as follows [31]:

$$\sigma_d = \underbrace{E \varepsilon_1 \exp \left[- \left(\frac{F}{F_0} \right)^c \right]}_{\substack{\text{Double factors of axial static load and dynamic load} \\ \text{(Considering damage)}}} - \underbrace{\sigma_s}_{\text{Axial static load factor}} + \underbrace{2\nu\sigma_3}_{\text{Confining pressure factor}} - \underbrace{(\beta_f p_f + \beta_m p_m)}_{\text{Gas pressure factor}} \quad (1)$$

where E represents the elastic modulus of coal, GPa, ε_1 represents axial strain, F represents the distribution variable of the strength of coal micro-unit, c and F_0 represent the characterization parameters of Weibull distribution, σ_s represents axial static load, MPa, ν represents Poisson's ratio of coal, σ_3 represents nominal stress, β_f represents effective stress coefficient of coal fracture, β_m represents effective stress coefficient of coal matrix, p_f represents the gas pressure of coal fracture, MPa, p_m represents the gas pressure of coal matrix pore, MPa.

(2) Gas desorption, diffusion, seepage, and emission equations

Based on the gas desorption, diffusion, and seepage equations in conditions of static stress, the migration equations were built by considering the gas emissions caused by dynamic load [32].

$$\begin{cases} V = \frac{V_L P_L p}{1 + P_L p} \\ \left(\frac{V_L \cdot P_L \cdot RT}{(P_m + P_L)^2} \cdot \frac{\rho_{gs}}{V_M} + \phi_m \right) \frac{\partial p_m}{\partial t} = - \left[p_m \cdot \frac{\partial \phi_m}{\partial t} + \frac{p_m - p_f}{\tau} \right] \\ \phi_f \frac{\partial p_f}{\partial t} + \nabla \cdot \left(- \frac{k \cdot p_f}{\mu} \nabla p_f \right) = \frac{p_m - p_f}{\tau} (1 - \phi_f) - p_f \frac{\partial \phi_f}{\partial t} \\ v' = -B \cdot p_i \cdot \sigma_i \cdot C^{\sigma_3} \cdot e^{-H\sigma_s} + D' \end{cases} \quad (2)$$

where V_L represents limit adsorption capacity, g/mL, P_L represents the relationship between gas pressure and gas adsorption capacity, MPa, p represents the gas pressure of the coal body, MPa, p_m represents gas pressure of coal matrix pore, MPa, ρ_{gs} represents the gas density, kg/m³, φ_m represents the porosity of coal matrix, p_f represents the gas pressure of coal fracture, MPa, p_m represents the gas pressure of coal matrix pore, MPa, φ_f represents fracture porosity, v' represents gas emission rate, p_i represents gas pressure in the sample, because the released gas directly comes from the free gas in the fracture, so here $p_f = p_i$, B , C , D' and H are constant, C is related to confining pressure, H is related to axial static load, B and D' are related to all loading conditions.

(3) Porosity and permeability control equations

As the link between solid mechanics and gas flow field, the porosity and permeability play the critical role. The changes in stress are the main reason for the changes in porosity and the fracture rate of coal, and finally result in gas migration. The porosity [33,34] and coal permeability evolution [35,36] were deduced as Equations (3) and (4).

$$\phi_f = 1 - \frac{1 - \phi_{f0}}{1 + \varepsilon_V} \left\{ \underbrace{1 - \frac{1}{K} [\beta_f (p_f - p_{f0}) + \beta_m (p_m - p_{m0})]}_{\text{Expansion deformation}} + \underbrace{\frac{\varepsilon_L p_m}{(p_m + P_L)(1 - \phi_{f0})}}_{\text{Adsorption expansion deformation}} \right\} \quad (3)$$

where ε_V represents volumetric strain of coal, $\varepsilon_z = \varepsilon_y + \varepsilon_x + \varepsilon_v$, Φ_{f0} represents initial porosity of coal, ε_L represents Langmuir volumetric strain constant.

$$k = k_0 \left\{ \frac{1}{\phi_{f0}} - \frac{1 - \phi_{f0}}{(1 + \varepsilon_V)\phi_{f0}} \left\{ \underbrace{1 - \frac{1}{K} [\beta_f (p_f - p_{f0}) + \beta_m (p_m - p_{m0})]}_{\text{Expansion deformation}} + \underbrace{\frac{\varepsilon_L p_m}{(p_m + P_L)(1 - \phi_{f0})}}_{\text{Adsorption expansion deformation}} \right\} \right\}^3 \quad (4)$$

where k_0 represents coal initial permeability; k represents coal permeability.

In the above model, the following assumptions also need to be made:

- (1) Gas seepage is not involved in the coal matrix, and gas diffusion is not involved in the coal seam, then it can also enter the adjacent rock strata. The gas pressure was the average measured value of 1.2 MPa.
- (2) The 4112 tunneling face has been excavated once, regardless of filling and supporting.
- (3) The average coal seam thickness in the corresponding local area of the accident site is the model's geological condition parameter.

3.2. Geometric Model and Boundary Conditions

According to the actual geological and mining environment of the 4112 working face, a two-dimensional geometric model of coal geology along the strike was established (length \times height is 160 m \times 60 m), as shown in Figure 2. To increase convergence, it was simplified appropriately, without considering the thickness change in the coal/rock strata and the internal tiny structure. Based on the on-site occurrence environment, the geometry model was established with the ratio of 1:1. Using this model, the stress distribution, coal/rock displacement and gas migration characteristics during coal seam mining were analyzed.

The established model of the 4112 working face included two parts: stress evolution and gas migration, and gas migration included gas diffusion and gas seepage, so it was necessary to set boundaries, respectively.

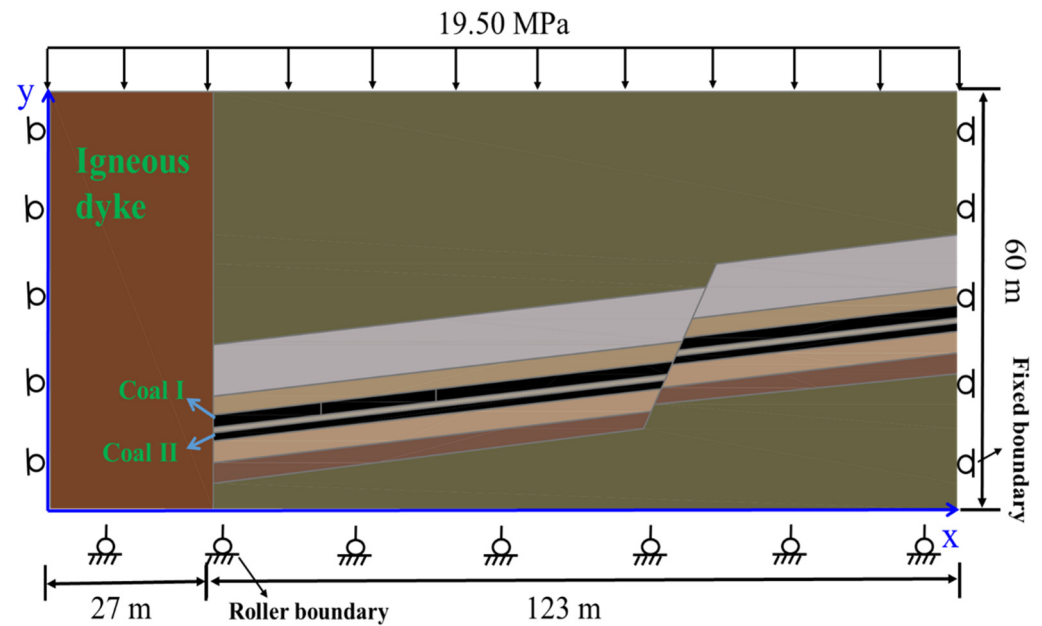


Figure 2. Geometry model of 4112 working face.

(1) Boundaries of the solid mechanics modules

Stress evolution mainly refers to the solid mechanics module. Due to the mining steps, three modules such as Solid, Solid 2, and Solid 3 were added to the Multiphysics model. The bottom of all solid mechanics models was set as a fixed boundary, and the left and right sides of the model were set to prevent horizontal displacement (Figure 2). Considering the designated load from the superimposed 780 m height stratum, a boundary load of 19.50 MPa was applied to the roof of the model (Figure 2). The boundary of the empty area after coal mining was a free boundary. To simulate the stress wave generated in the complex stope environment, the dynamic load was applied to the coal–rock junction at the fault, which was located at the front of the 4112 working face. The dynamic load generated by the earthquake source could be calculated by Equation (5):

$$S(t) = \sigma_a R(t) \quad (5)$$

where σ_a is the stress peak value, $R(t)$ is the Ricker wave function.

Based on the method of calculating apparent stress in earthquakes [37], the stress peak value was expressed as follows:

$$\sigma_a = \frac{GE_R}{M_0} \quad (6)$$

where G represents rock mass shear modulus, GPa; E_R represents radiant energy, J; M_0 is the earthquake moment, Mm. According to Polish empirical formula [38], there is the following relationship between earthquake moment M_0 and magnitude M_e :

$$\lg M_0 = 10.42 + 1.009 M_e \quad (7)$$

The radiant energy E_R could be calculated by the Gutenberg–Richter formula [39]:

$$\lg E_R = 1.5 M_e + 4.8 \quad (8)$$

Wavelet is a common waveform in earthquake wave simulation, with short duration and fast convergence. The Ricker wave function is shown as follows:

$$R(t) = \left[1 - 2(\pi f_0 t)^2\right] e^{-(\pi f_0 t)^2} \quad (9)$$

where f_0 is the main frequency, Hz.

The expression of dynamic load generated by the vertical earthquake in Equations (3)–(8) could be expressed as follows:

$$S(t) = G \left[1 - 2(\pi f_0 t)^2 \right] e^{-(\pi f_0 t)^2} \times 10^{0.491 M_e - 5.62} \quad (10)$$

From Equation (10), the dynamic load was determined by the frequency and magnitude of the stress wave generated by the earthquake source. According to the on-site damage and Rayleigh mechanical damping form, the frequency of the dynamic load was 50 Hz and the magnitude was 10.5 level. The dynamic load stress wave in this simulation is shown in Figure 3.

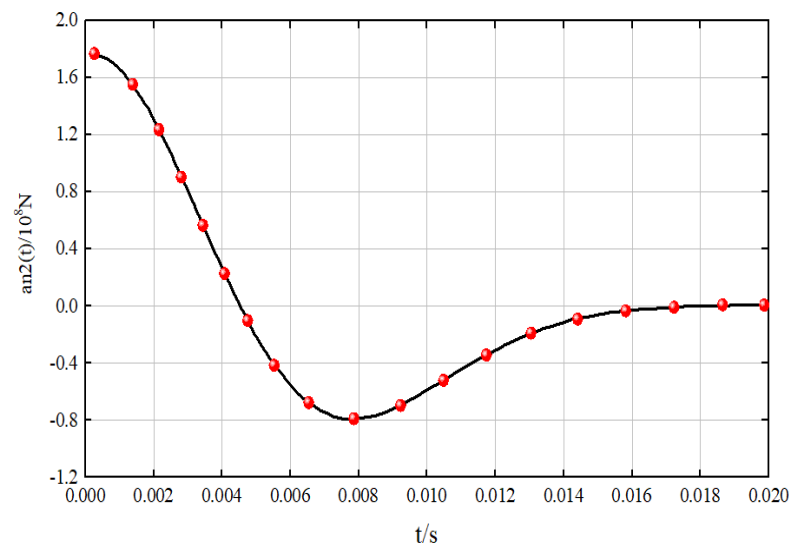


Figure 3. Stress wave of dynamic load.

(2) PDE module

The gas diffusion field is controlled by the user-defined partial differential equation (PDE). Gas diffusion only occurs in coal seams; the coal bed surrounding the boundary was set as the first boundary condition, and the gas pressure at the boundary had the initial value of P_0 . The coal bed initial gas conditions are expressed as follows:

$$\begin{cases} p_m(0) = p_0 \\ \frac{\partial p_m}{\partial t} = 0 \end{cases} \quad (11)$$

where P_0 represents the initial gas pressure value in the solution domain.

The gas seepage field is also controlled by the self-defined partial differential equation (PDE2). The gas seepage not only occurred in the coal seam, but also flowed into the rock stratum and continued to seep into the rock stratum. Therefore, the initial condition of rock stratum gas pressure was established as the barometric pressure value of 0.1 MPa, and the gas pressure around the whole coal model was set as 1.20 MPa to simulate the gas from infinite distance. The boundaries of gas pressure in the model are shown in Figure 4. The initial conditions of the coal seepage field are expressed as Equation (12).

$$\begin{cases} p_f(0) = p_0 \\ \frac{\partial p_f}{\partial t} = 0 \end{cases} \quad (12)$$

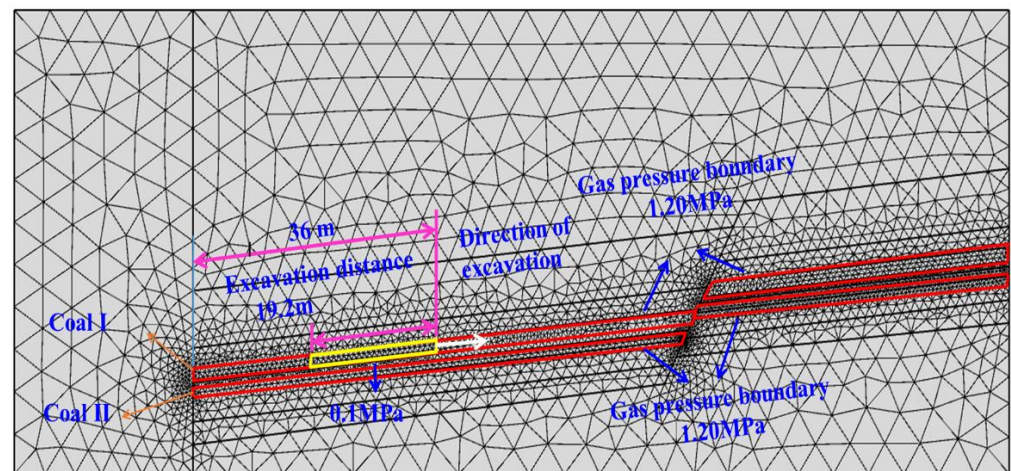


Figure 4. Boundary conditions and mesh division.

3.3. Mesh Division and Solution Settings

To ensure the accuracy of the numerical solution, it is critical to select the appropriate method of mesh division. In this model, the triangular unit was used to mesh the whole area; to ensure the accuracy of the results, extremely refined grids were used for the coal seam area, while refined grids were used for the remaining areas. The specific results are as follows in Figure 4.

After meshing, a solution method needed to be selected to obtain the numerical results. Because there were five modules in the Multiphysics, multi-solvers and multi-steps were designed, as shown in Figure 5. First, the Solid module was solved in a steady state, and the initial stress distribution without excavation was calculated. Second, the Solid 2 module was used to solve the stress distribution after coal mining, and the steady-state solution mode was still adopted. Finally, the transient solution of Solid 3, PDE and PDE 2 was carried out, in which the external stress of Solid 3 was imported from the calculation result of Solid 2, and the boundary of the hollowed-out area in Solid 3 was set as the low reflection boundary. The coupling solution of dynamic load in Solid 3, gas diffusion in PDE and gas seepage in PDE 2 could be realized, through which the gas-bearing coal seam stress and gas induced by dynamic load in the complex geological environment would be obtained.

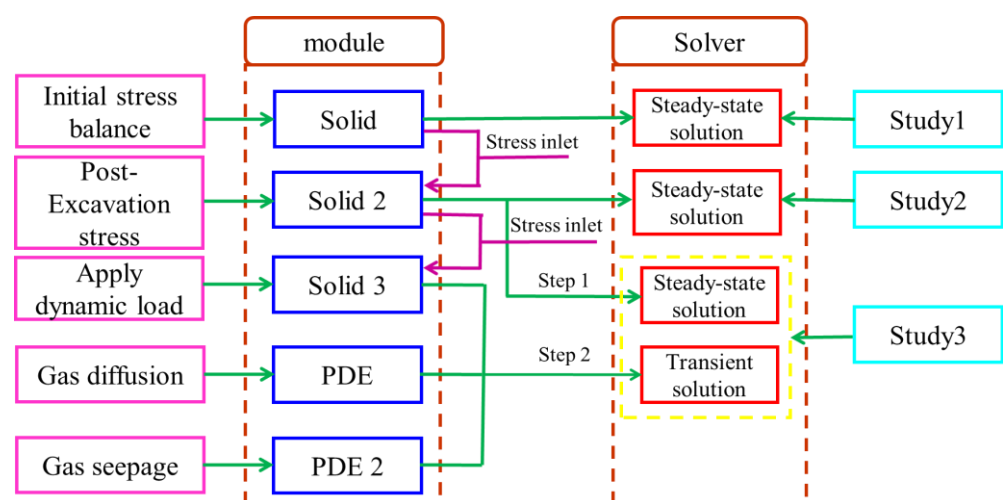


Figure 5. Multi-solvers and multi-steps mode.

3.4. Initial Parameters

The assignment of coal strata mechanical parameters and gas basic parameters was the joint goal of the numerical simulation. Based on the analysis results of the coal/rock basic

parameters under the 4112 working face and the measurement results of the coal seam gas parameters, the mechanical parameters and basic gas parameters were determined, as shown in Tables 1 and 2.

Table 1. Coal/rock parameters.

Name	Rock Character	Elastic Modulus (GPa)	Poisson's Ratio	Density (kg/m ³)	Cohesive Force (MPa)	Angle of Internal Friction (deg)
Main roof I	Medium white siltstone	9.50	0.25	2700	12.3	29
Direct roof of coal I	Grey black siltstone	7.80	0.23	2600	10.5	27
Coal seam I	Coal	1.20	0.20	1500	2.0	30
Coal floor I	Grey black siltstone	7.80	0.23	2600	10.5	27
Coal II	Coal	1.20	0.20	1500	2.0	30
Coal direct bottom II	Grey brown fine medium sandstone	11.30	0.28	2717	17.0	25
Hard floor II	Black sand shale	26.00	0.33	2700	27.2	28
Igneous wall	Igneous rock	28.00	0.17	2800	12.6	39
Other rock mass	Medium sandstone	13.00	0.30	2717	19.0	25

Table 2. Gas parameters.

Parameter	Value	Parameter	Value
Initial porosity of coal I sample, Φ_{01}	0.3	Limit adsorption capacity, V_L	0.02
Initial permeability of coal I sample, k_{01}	$2.5 \times 10^{-15} \text{ m}^2$	Methane Langmuir adsorption pressure constant, P_L	1
Initial porosity of coal II sample, Φ_{02}	0.3	The molar volume constant of gas in standard state, V_M	22.4 L/mol
Initial permeability of coal II sample, k_{02}	$2.5 \times 10^{-15} \text{ m}^2$	The density of gas in standard state, ρ_{gs}	0.717 m ³ /kg
Initial porosity of rock mass, Φ_{0r}	0.01	The molecular weight of methane, M_g	16 g/mol
Initial permeability of rock mass, k_{0r}	$3 \times 10^{-20} \text{ m}^2$	Universal gas constant, r	8.314 J/(mol/K)
Initial gas pressure of coal matrix, P_{m0}	1.20 MPa	Simulated field temperature, T	293.1 K
Initial gas pressure of coal fissure, P_{f0}	1.20 MPa	Dynamic viscosity of gas molecules, μ	$1.84 \times 10^{-5} \text{ Pa}\cdot\text{s}$
Gas pressure in rock, P_{r0}	0.10 MPa	Muir volume strain constant, ϵ_L	0.012
Muir volume constant, b_1	1.84×10^{-3}	Muir pressure constant, b_2	$1/16 \times 10^{-171} \text{ /Pa}$

4. Results and Discussion

4.1. Stress Distribution

4.1.1. Stress Distribution of Roadway without Excavation

Firstly, the stress distribution near the 4112 roadway was calculated when the roadway was not excavated, as shown in Figure 6. By reshaping the geological conditions around the 4112 roadway, the effects of the igneous wall and fault could be considered. In the whole numerical model, there were two stress anomaly areas, one was the fault area in front of the 4112 roadway, and the stress anomaly area was distributed following the normal orientation of the fault plane; the highest abnormal stress in this area was $4.5 \times 10^7 \text{ Pa}$, and the average abnormal stress in the area was $3.7 \times 10^7 \text{ Pa}$. The other was the rear igneous wall area, and the stress anomaly area extended downward along the coal seam's direction of inclination; the highest abnormal stress in this area was $4.1 \times 10^7 \text{ Pa}$, and the average abnormal stress in the area was $3.3 \times 10^7 \text{ Pa}$.

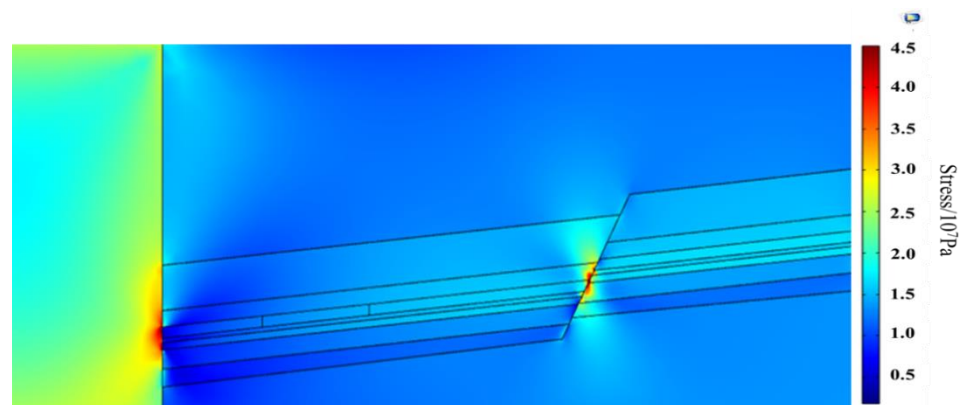


Figure 6. Initial stress equilibrium.

Comparing and analyzing the abnormal stress zone with the normal stress zone, the abnormal stress was about 2–3 times the normal stress. The abnormal stress in the visible fault and structural areas provided the starting stress for coal and gas outbursts in this accident. The uneven distribution of stress and the intrusion of faults/igneous rocks were the main factors causing the original stress anomaly in the area.

4.1.2. Stress Distribution after Roadway Excavation

After the original stress balance, the stress distribution results after the excavation of the 4112 roadway were calculated. This result did not consider the influence of dynamic load, so Figure 7 reflects the influence of excavation on the stress distribution of coal and rock mass in this area. After 19.2 m of tunneling in the roadway, the stress concentration areas were formed before the tunneling head and behind the open-off cut; then, stress relief areas were formed near the roof of the roadway. The peak stress in the abnormal stress area at both ends, before and after excavation, was 2.8×10^7 Pa, with an average stress of 2.4×10^7 Pa. There was a significant decrease in stress in the stress-release area of the roof, and the stress distribution in the release area was relatively stable, with an average value of 0.7×10^7 Pa.

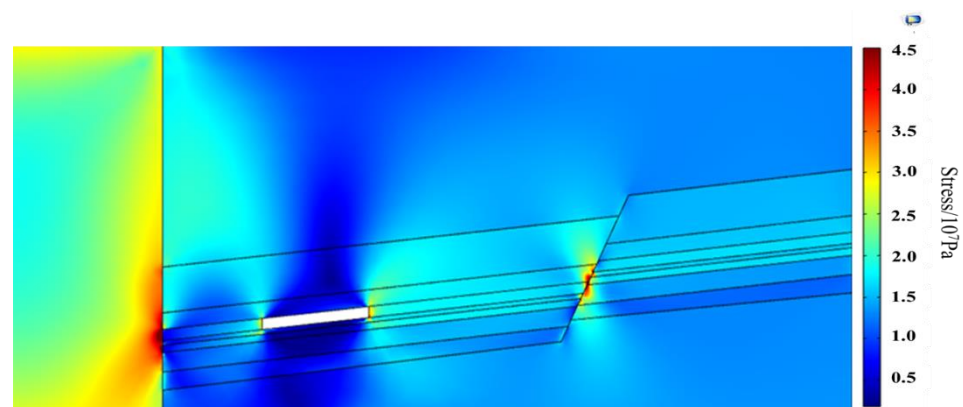


Figure 7. Stress distribution after roadway tunnelling.

The reason for the above phenomenon is because the coal body was excavated to form an empty area, the overlying rock mass on the roof was regarded as a fixed beam at both ends, and its weight was mainly supported by the solid coal before the tunneling head and behind the open-off cut. Therefore, the concentration of stresses before and after the tunneling area and pressure relief from top to bottom would be formed. Moreover, comparing Figures 6 and 7, the 4112 roadway excavation had a slight impact on the stress in the two structural areas, and it had a greater impact on the stress in the igneous intrusion area, mainly because the igneous rock was relatively closer to the current excavation area.

4.1.3. Stress Distribution of Gas-Bearing Coal under Dynamic Load Disturbance

The evolution law of dynamic load caused by fault slip is shown in Figure 8; in the complicated geological structure, the driving induced the active slip of the fault before the working face to generate a huge dynamic load, which spreads in coal/rock mass in the form of stress wave.

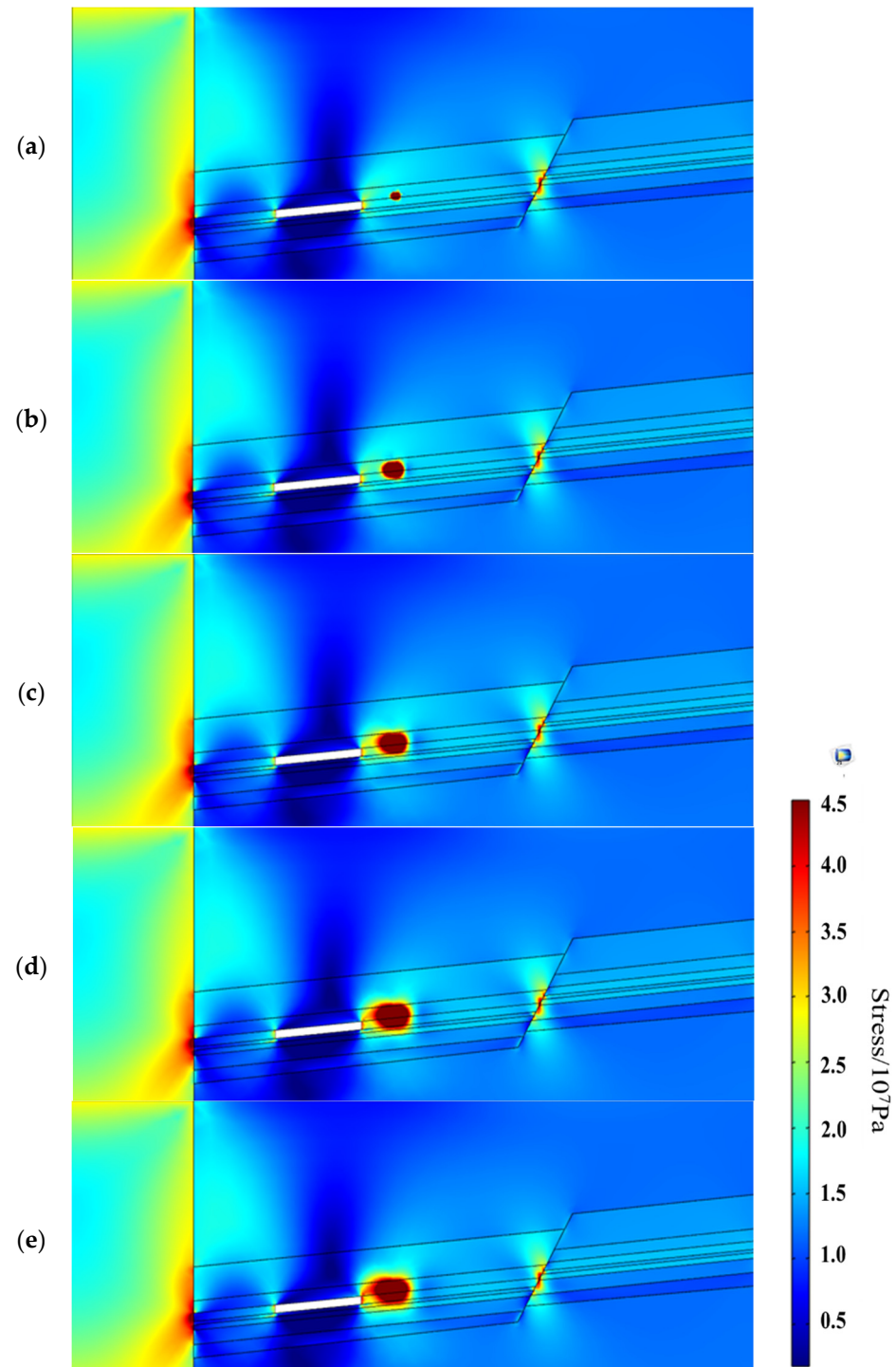


Figure 8. Stress evolution during the stress propagation induced by dynamic load. (a) Stress distribution at 0.2 ms, (b) stress distribution at 1 ms, (c) stress distribution at 4 ms, (d) stress distribution at 6 ms, (e) stress distribution at 7 ms.

The dynamic load was generated at 0.2 ms, and the maximum abnormal stress near the source could reach 4.5×10^7 Pa. As time passed, the dynamic load gradually radiated to both sides of the source, and the stress magnitude did not decay during the propagation process, maintaining a strength of around 4.5×10^7 Pa. At 7 ms, the propagation of the dynamic load basically stopped.

Compared with static load and tectonic stress, the dynamic load was much larger, so the stress wave showed the abnormal stress phenomenon everywhere it passed, and caused more severe damage to the coal body along the way. Moreover, during the gradual propagation of stress waves towards both sides, the dynamic stress anomaly zone gradually encountered the static stress anomaly zone mentioned earlier, causing the coal body at the upper end of the excavation face to be subjected to a strong load impact, a gradually breaking and protruding phenomenon.

4.2. Displacement Distribution

The distribution pattern of the coal displacement is shown in Figure 9. When the stress waves propagated towards both sides of the earthquake source, the coal body was subjected to a strong dynamic impact greater than its strength, leading to the accumulation of elastic potential energy inside the coal body and the occurrence of fragmentation.

Due to the attenuation of energy propagation, the energy accumulated along the coal body gradually decreased, and the displacement also decreased. The coal body at the source had the maximum displacement. The displacement at the source occurred at 1 ms, with a small displacement of 0.3 m. As the energy accumulated further, the displacement at the source gradually increased to 0.8 m, and the displacement range further expanded. At 10 ms, it propagated to the coal wall, causing strong displacement of the coal along the way.

In the meanwhile, as time went on, the overall displacement of the coal experienced changes, first increasing and then decreasing. Under the action of the stress wave, the coal gradually moved out to find a breakthrough. When the abnormal stress area caused by dynamic load coincided with the abnormal stress area before the coal wall, the larger stress destroyed the coal wall which then fell onto the roadway. This process had a certain degree of lag compared to the propagation of stress waves, mainly because the displacement of coal absorption energy had a time effect. In the early stages of the loading process, the coal converted the loaded energy into internal energy and accumulated it inside. When the received energy was greater than the strength of the coal, the internal energy caused coal damage, and the accumulated elastic potential energy became the driving force for the coal outburst.

4.3. Gas Migration

Under the influence of the complex stress fields, the coal body was broken or even crushed under the action of dynamic load, then massive amounts of gas in the coal matrix was desorbed, which caused a rise in fracture gas pressure in the area affected by dynamic load. It was precisely because a great quantity of gas was desorbed in a few seconds, when the broken coal body crashed through the coal wall, the gas moved rapidly to the roadway at the same time, leading to the gas overrun of the roadway and even the gas backflow phenomenon.

As Figure 10 shows, during the course of the accident, the changes in gas pressure had a spatiotemporal effect. The gas pressure rapidly increased in the initial stages of the accident, and then gradually decreased over time. This is because when the dynamic load had an impact on the coal body, it promoted the rapid desorption of adsorbed gas in the coal matrix into a free state, leading an increase in gas pressure, reaching its peak at 6 ms. As the coal body was further impacted, free gas escaped to the outside of the coal body, and the gas inside the coal body gradually released to the outside., the gas pressure inside the coal body then gradually decreased.

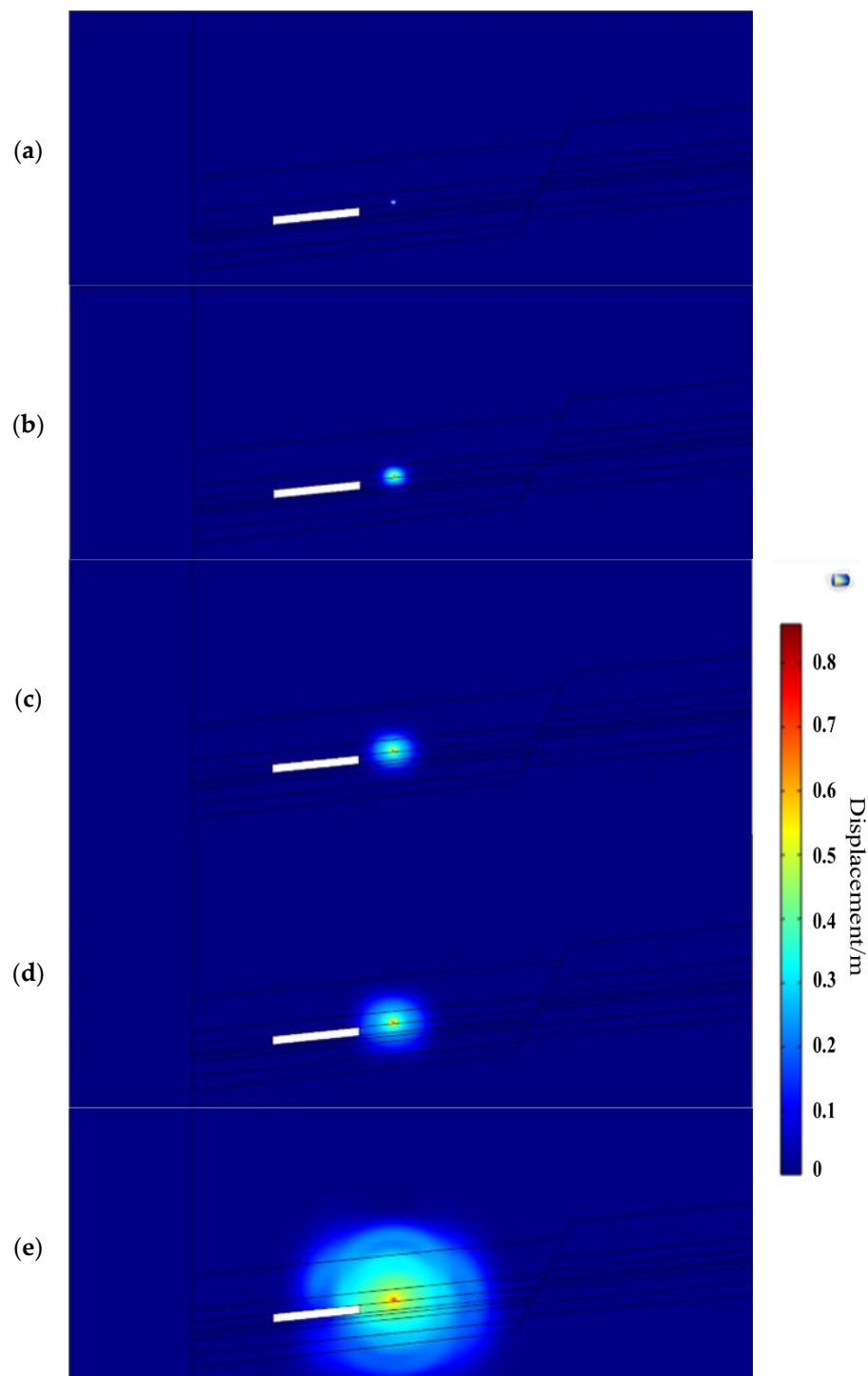


Figure 9. Displacement evolution induced by dynamic load. (a) Displacement distribution at 1 ms, (b) displacement distribution at 3 ms, (c) displacement distribution at 7 ms, (d) displacement distribution at 9 ms, (e) displacement distribution at 10 ms.

With the distance changed, the gas pressure increased first and then decreased, and decreased along the center of the earthquake source towards both sides. According to the trend in the gas pressure change, the gas migration zone can be divided into three stages: gas reduction stage, gas accumulation stage, and original gas pressure stage. A natural gas anomaly area was formed at 8.5 m from the working face, where the natural gas pressure was greater than the accumulation stage. When the impact load continued to act on the coal

body, the gas pressure in the peak area was greater than the coal body's bearing capacity, ultimately leading to a large amount of gas outburst.

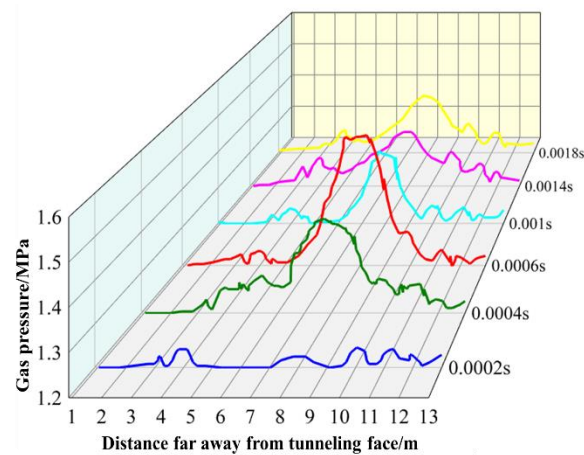


Figure 10. Gas pressure distribution.

4.4. Coal Seam Porosity and Permeability Evolution

The stress field and gas field of the gas-bearing coal interacted with each other, and the change in coal porosity was the result of the coupling effect between them. Due to the influence of multifield coupling effects, gas-bearing coal undergoes degradation effects internally, which greatly increase coal porosity and provide an advantageous channel for gas desorption in the coal matrix.

As shown in Figure 11, the porosity of the coal near the earthquake source increased the most, and the porosity increased gradually with the outward radiation direction of stress wave. In addition, the porosity rapidly increased during the short period from stress wave generation to propagation, reaching its peak at 6 ms. The maximum porosity in the central area was 2.2 times that of the original porosity, with a maximum of 0.22. When the stress wave energy diffused outward, although the porosity of coal in the central area of the earthquake source decreased, due to the irreversibility of the coal degradation effect, the porosity at the center was still close to 1.9 times the original porosity, providing a basis for subsequent gas outbursts. The increase in porosity expanded the internal migration space of the coal, providing more effective channels for gas migration, correspondingly increasing the permeability of the coal, promoting rapid gas release into the tunnel, and causing the gas to exceed the limit in the tunnel.

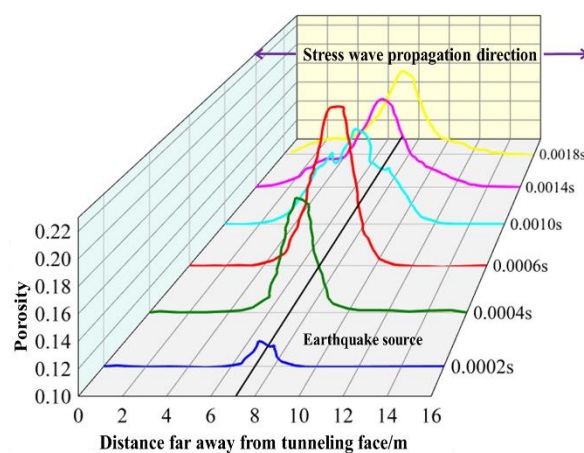


Figure 11. Porosity evolution of coal seam.

The permeability of gas-bearing coal being influenced by dynamic load is shown in Figure 12. The permeability and porosity of coal obey approximately the same law, with

the maximum increase in the center of the earthquake source, and the maximum increase in the permeability of coal in 6 ms reaching about 1.6 times the original permeability. Along the propagation direction of the stress wave, the increase in the amplitude of permeability decreased gradually. The permeability increased first and then decreased to a stable value with the propagation time of the stress wave, and the stable permeability was about seven times that of the original permeability.

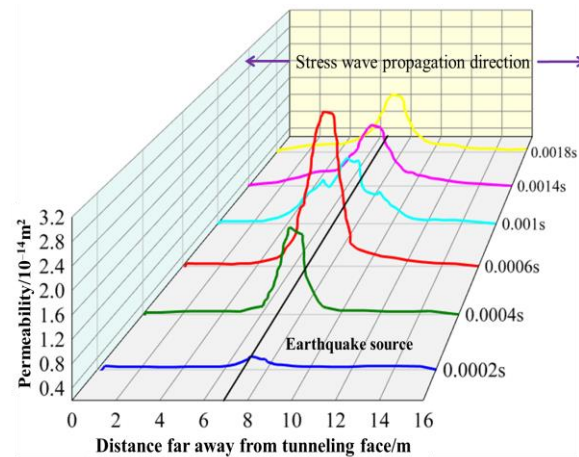


Figure 12. Permeability evolution of coal seam.

5. Coal and Gas Outburst Case Analysis

5.1. Coal Outburst in Accident Field

The influence of stress distribution had an obvious dynamic effect on this accident. In this accident, a large amount of coal was thrown out, and the total length of the roadway covered by the coal rock was 26 m. The thickness of the third outburst prevention door was 0.4 m. The third outburst prevention door was 5.7 m in from the working face. The outburst filled the roadway, less than 0.5 m from the top of the U-shaped steel shed center, and about 293 t of coal and rock was displaced. The outburst included large gray-black rocks, massive high metamorphic coal and broken coal, and the separation was not obvious. The large rock was black fine sandstone, the rock had a jointed surface, and the contact surface between the rock and the coal was smooth, as shown in Figure 13. It was identified by the geological mine personnel as the coal layer I false roof/direct roof.



Figure 13. Accident scene. (a) Outburst coal body, (b) outburst rock body.

After the accident, the end of the air duct was bent, and the 26th shed at the head was tilted and poured into the coal pile. The upper part of the 25th was close to the 24th, and the connecting rods of the 23rd and 22nd, 22nd and 21st sheds were bent, as shown in Figure 14.



Figure 14. Destruction of U shape support. (a) Anchor rod failure situation, (b) anchor network damage situation.

According to the accident report, when the accident occurred, the coal body near the excavation face was the first to break and spray out in large quantities, and the support above the roadway in that area was the most severely damaged. According to the above simulation results, it can be concluded that this accident was caused by an increase in abnormal stress due to stress connectivity, and the abnormal stress zone appeared at the upper end of the coal body in the excavation face, gradually spreading towards both ends. This led to a significant displacement of the coal body at the upper end of the excavation face, ultimately resulting in a significant protrusion of the coal rock mass.

By comparing the stress and displacement distribution results in the numerical simulation with the phenomena of coal outburst and support failure on site, it was found that the numerical simulation results were highly consistent with the actual situation on site, indicating that the results in this part of the numerical simulation are true and reliable.

5.2. Gas Migration of Accident Field

The influence of gas migration has been shown before the accident. Two days before the accident, the coal seam was soft, the coal wall spalling was more than 500 mm, and the ground pressure was obvious. Although there was no gas overrun phenomenon, the gas pressure had increased significantly. The monitoring results from the gas detector had undergone irregular changes. Massive amounts of gas gushed out during this accident, and the phenomenon of a gas countercurrent was produced. The gas emission was 11,232 m³, and the gas emission per ton of coal was 38.3 m³.

According to the on-site accident situation, before the accident, the coal seam near the coal wall gradually became soft and collapsed. This is clearly due to the dynamic load damaging the coal body, causing a rapid increase in the porosity and permeability of the coal body, resulting in a decrease in density. This phenomenon is highly consistent with the evolution of porosity and permeability in the numerical simulation results.

The increase in gas pressure in this area indicated that the adsorbed gas in the coal seam matrix had undergone desorption, becoming free gas filling the coal seam pores. After the accident, gas exceeding the limit first occurred near the coal wall, and the escaping gas quickly filled the roadway. Based on the numerical simulation analysis, it is known that before the accident, the gas had undergone desorption and migrated to the cracks in the coal body, causing a sharp increase in gas pressure, leading to coal fragmentation and an increase in permeability. Due to the dynamic influence of the gas pressure, a large amount of gas was rapidly discharged, and the migration of the gas in the coal is shown in Figure 15. By comparing and analyzing the pressure evolution law in the numerical simulation with the gas outburst characteristics at the accident site, it was found that the pressure evolution law reflected in the simulation was the same as the actual situation on site, indicating that the content in this part of the numerical simulation results is true and reliable.

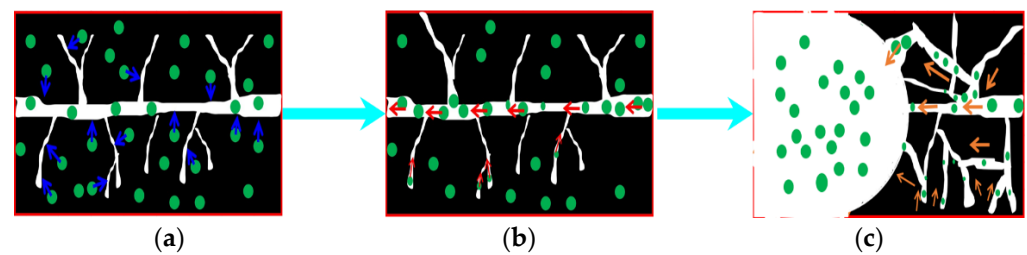


Figure 15. Process of gas migration. (a) Matrix gas desorption, (b) fissure gas seepage, (c) coal seam gas outburst.

5.3. Mine Safety and Sustainable Development

Based on the above numerical simulation and field analysis results, it can be seen that the coal and gas outburst disaster was mainly caused by the combined action of an abnormal in situ stress load and abnormal gas pressure. The dual action promoted the destruction of the coal and rock mass properties in the outburst area, and satisfied the multi-factor conditions of coal and gas outburst. Under the action of high in situ stress and high gas pressure, the release of the elastic potential of the coal and rock mass led to the instability and fracture of the coal body, which subsequently led to gas desorption and expansion. The gas was quickly released, breaking and ejecting the body of coal, resulting in the coal and gas outbursts.

In order to promote the safe mining of coal and maintain the sustainable development of the coal economy and the environment, it is necessary to carry out prevention and control measures for coal and gas outbursts for the whole process of coal mining [40–42], according to the formation mechanisms and evolution processes of coal and gas outbursts, as shown in Figure 16.

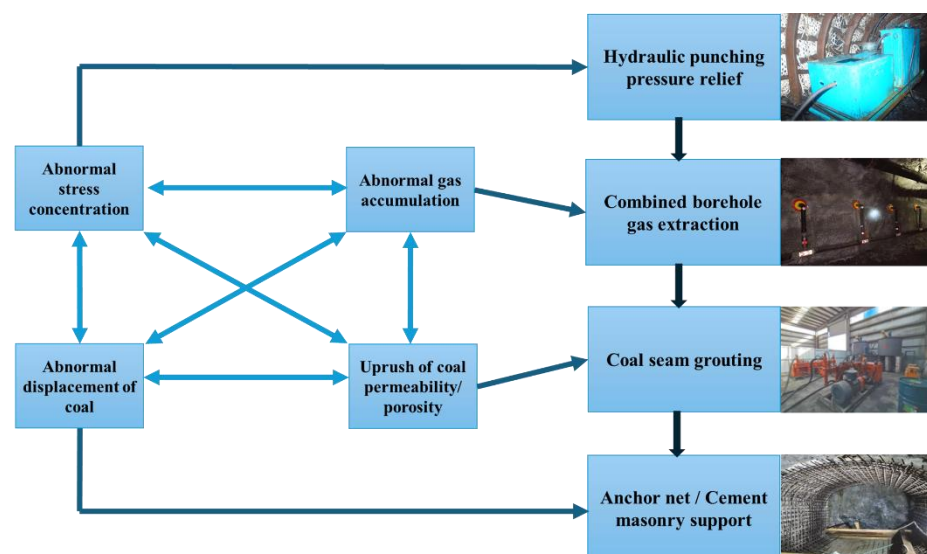


Figure 16. Mechanism diagram of prevention and control measures.

- (1) In order to release the stress in the coal seam in advance, the stress concentration area should be transferred to the deep; to reduce the damage and impact of abnormal ground stress and dynamic loads on the coal body, hydraulic punching should be carried out on the igneous rock wall and fault area before mining to relieve pressure and discharge the coal body. The problem of abnormal gas accumulation caused by complex geological conditions could be solved by increasing the stress concentration range and weakening the stress concentration degree after deep and shallow hole alternate blasting. When the working face starts to advance, advance pressure relief hydraulic punching should be carried out in the excavation head area with the mining

progress, so as to ensure the timely release of excavation stress, and avoid greater damage to the coal body caused by the superposition of dynamic stress waves and ground stress.

- (2) When the coal seam is impacted by stress waves, a large amount of residual gas in the coal body is released from the coal matrix, leading to serious gas outbursts. In order to reduce the risk of harm from gas outbursts, it is necessary to start from the gas reserves in the coal seams. Before coal seam mining, a combined borehole is used for gas pre-extraction. Gas drainage can greatly reduce gas pressure, lower the internal energy of the gas, and reduce the probability of gas outbursts during abnormal accumulation.
- (3) The abnormally increased stress has a destructive effect on the coal body, resulting in a gradual decrease in the porosity and permeability of the coal body from the center of the source to both sides. To enhance the strength and increase the porosity and permeability of the coal body, a grouting measure is adopted to modify the coal body, so that it penetrates the cracks and pores of the coal seam. After solidification, the cracks and pores in the coal seam are filled and sealed to improve the mechanical strength, inhibit gas desorption, and increase the energy required for coal fracture so that the adsorbed gas in the coal seam cannot quickly become free gas, thus preventing the compressed gas potential from turning into outburst kinetic energy when the coal seam is destroyed. Solidifying the bond also improves the strength and changes the physical and mechanical properties of the outburst coal seam, so as to achieve the purpose of preventing coal and gas outbursts.
- (4) According to the characteristics of displacement distribution, the migration of coal and rock mass is related to the stress wave propagation distance caused by the main dynamic load. In order to ensure the maximum support strength, the whole roadway should be supported by the anchor net before advancing the working face, and then the focus area of the dynamic load and the position along the stress wave are reinforced by the support method of masonry concrete. In this way, when the impact load is greater than the strength of the coal body, the coal body can still be supported and restrained in the upper part of the roadway, so as to avoid damage to the roadway caused by coal ejection during coal and gas outbursts, which would disrupt the sustainability of coal mine development.

To verify the effectiveness of these disaster prevention and control measures, multiple monitoring techniques can be used to analyze disaster parameters. Firstly, based on the methane sensor in the tunnel, real-time monitoring of methane concentrations in the environment can be carried out to ensure that the gas concentration in the tunnel does not exceed the limit. Secondly, two methods are used to quantitatively evaluate the gas content in coal seams, namely, the gas emission and gas desorption parameters from drilling cuttings. In addition, microseismic monitoring technology is used to monitor the microfracturing activity in coal seams, indirectly analyzing the real-time stress damage situation inside coal seams. At the same time, force sensors and roof displacement monitoring technology are used to monitor the stress and displacement in coal seams, directly analyze the displacement of coal seams, and clarify the characteristics of tunnel failure.

Based on the comprehensive effect of combining four measures, this set of measures can reduce the probability of stress and abnormal gas pressure accumulation leading to accidents during coal roadway excavation, thereby improving the sustainability and safety of coal mines.

6. Conclusions

Based on the multifield coupling model for the impact damage of gas-bearing coal, this study analyzed the characteristics and causes of major coal and gas outburst accidents in the 4112 roadway and drew the following conclusions.

- (1) The complex geological and deep mining conditions were the main prerequisites for the accident. Before the accident, there was a noticeable vibration sound, indicating

the presence of dynamic loads nearby. The complex geological structure and mining activities led to the sliding of the fault ahead, resulting in severe dynamic loads, which directly caused this accident.

- (2) The stress propagates outward from the center of the earthquake source, and during the propagation process, the energy continues to decay. Therefore, the displacement of the coal body at the center of the seismic source was maximum, and the displacement of the coal body from the center of the earthquake source to the outside gradually decreased. When the stress propagated to the stress concentration area in front of the coal wall of the excavation head, the superposition of dynamic and static stresses would increase the stress in that area, exceeding the load that the coal body could bear, damaging the coal wall and causing the gas and coal inside to be discharged together into the tunnel.
- (3) The dynamic load caused the coal to quickly break, promoted gas desorption, and led to a rapid increase in gas pressure near the seismic source. At the same time, it increased the porosity and permeability of the coal, providing a channel for rapid gas migration. Ultimately, it led to a gas outburst, resulting in the gas backflow phenomenon.
- (4) By comparing and analyzing the numerical simulation results with the actual situation on site, a four-in-one, full process coal and gas outburst prevention and control measure is proposed, based on the evolution characteristics of the accident. Through measures of pre-disaster prevention and post-disaster reduction, the probability of accidents in coal mines is reduced while increasing their disaster resistance and providing theoretical support for the sustainability of safety in coal mining production.

Author Contributions: Methodology, X.K.; formal analysis, X.K. and D.H.; investigation, T.Z. and Y.C.; resources, X.K.; writing—original draft preparation, X.K. and T.Z.; writing—review and editing, X.K. and T.Z.; supervision, D.H. All authors have read and agreed to the published version of the manuscript.

Funding: This research was funded by the National Natural Science Foundation of China (Grant No.51904236, Grant No.52204235), Natural Science Basic Research Program of Shaanxi (2020JQ-756), China Postdoctoral Science Foundation (2021M693879), Excellent Youth Program of Xi'an University of Science and Technology.

Institutional Review Board Statement: Not applicable.

Informed Consent Statement: Not applicable.

Data Availability Statement: The data used to support the findings of this study are available from the corresponding author.

Conflicts of Interest: The authors declare no conflicts of interest.

References

1. Zhang, W.; Feng, P. Differentiation research of CO₂ emissions from energy consumption and their influencing mechanism on the industrial enterprises above designated size in Chinese industrial cities: Based on geographical detector method. *Nat. Hazards* **2020**, *102*, 645–658. [\[CrossRef\]](#)
2. Fauchille, A.; Hedan, S.; Valle, V.; Pret, D.; Cabrera, J.; Cosenza, P. Multi-scale study on the deformation and fracture evolution of clay rock sample subjected to desiccation. *Appl. Clay Sci.* **2016**, *132*, 251–260. [\[CrossRef\]](#)
3. Knapp, M.; Scheidweiler, L.; Külheim, F.; Kleinschek, R.; Necki, J.; Jagoda, P.; Butz, A. Spectrometric imaging of sub-hourly methane emission dynamics from coal mine Ventilation. *Environ. Res. Lett.* **2023**, *18*, 4. [\[CrossRef\]](#)
4. Soleimani, F.; Si, G.; Roshan, H.; Zhang, Z. Numerical modelling of coal and gas outburst initiation using energy balance principles. *Fuel* **2023**, *334*, 126687. [\[CrossRef\]](#)
5. Dutka, B. Effect of depth on the sorption capacity of coals affected by outburst hazard. *Fuel* **2021**, *306*, 121611. [\[CrossRef\]](#)
6. Kursunoglu, N.; Onder, M. Application of structural equation modeling to evaluate coal and gas outbursts. *Tunn. Undergr. Space Technol.* **2019**, *88*, 63–72. [\[CrossRef\]](#)
7. Filippo, M.; Ioannis, S.; Paolo, V.; Victor, M.B. Rocking response of inverted pendulum structures under blast loading. *Int. J. Mech. Sci.* **2019**, *157–158*, 833–848. [\[CrossRef\]](#)

8. Yang, K.; Lei, Y.; Chen, W.; Liu, L. Carbon dioxide emission reduction quota allocation study on Chinese provinces based on two-stage Shapley information entropy model. *Nat. Hazards* **2018**, *91*, 321–335. [[CrossRef](#)]
9. Liu, Y.; Zhao, H.; Liu, S.; Sun, W. Asymmetric damage mechanism of floor roadway based on zonal damage characteristics of longwall panel floor: A case study. *Nat. Hazards* **2022**, *114*, 1015–1041. [[CrossRef](#)]
10. Wang, C.; Guo, E.; Cao, Y.; Zhang, H.; Zhang, Y. Statistical characteristics of production safety accidents and its strategy implications for administrators in Inner Mongolia. *Nat. Hazards* **2023**, *117*, 745–762. [[CrossRef](#)]
11. Bartosz, D.; Renata, K.; Klas, A. Current status of carbon capture, utilization, and storage technologies in the global economy: A survey of technical assessment. *Fuel* **2023**, *342*, 127776. [[CrossRef](#)]
12. Danesh, N.; Zhao, Y.; Teng, T.; Masoudian, M.S. Prediction of interactive effects of CBM production, faulting stress regime, and fault in coal reservoir: Numerical simulation. *J. Nat. Gas. Sci. Eng.* **2022**, *99*, 104419. [[CrossRef](#)]
13. Yu, M.; Yang, N.; Li, H.; Wang, L.; Wu, M.; Wang, F.; Chu, T.; Wang, K. Numerical investigation on the effects of axial-stress loads on the temperature-programmed oxidation characteristics of loose broken coal. *Energy* **2024**, *289*, 129974. [[CrossRef](#)]
14. Zhao, Y.; Lin, B.; Liu, T.; Zheng, Y.; Li, Q.; Song, R. Mechanism of multifield coupling-induced outburst in mining-disturbed coal seam. *Fuel* **2020**, *272*, 117716. [[CrossRef](#)]
15. Yang, T.; Xu, T.; Liu, H.; Tang, C.; Shi, B.; Yu, Q. Stress–damage–flow coupling model and its application to pressure relief coal bed methane in deep coal seam. *Int. J. Coal Geol.* **2011**, *864*, 357–366. [[CrossRef](#)]
16. Wang, D.; Wei, J.; Qin, H.; Wei, L. Research on Solid-Gas Coupling Dynamic Model for Loaded Coal Containing Gas. *Adv. Mat. Res.* **2012**, *594–597*, 446–451. [[CrossRef](#)]
17. Liu, T.; Lin, B.; Yang, W.; Liu, T.; Kong, J.; Huang, Z.; Wang, R.; Zhao, Y. Dynamic diffusion-based multifield coupling model for gas drainage. *J. Nat. Gas. Sci. Eng.* **2017**, *44*, 233–249. [[CrossRef](#)]
18. Xue, S.; Wang, Y.; Xie, J.; Wang, G. A coupled approach to simulate initiation of outbursts of coal and gas: Model development. *Int. J. Coal Geol.* **2011**, *862*, 222–230. [[CrossRef](#)]
19. Wang, K.; Wang, Y.; Xu, C.; Guo, H.; Xu, Z.; Liu, Y.; Dong, H.; Ju, Y. Modeling of multi-field gas desorption-diffusion in coal: A new insight into the bidisperse model. *Energy* **2023**, *267*, 126534. [[CrossRef](#)]
20. Gao, K.; Liu, Z.; Liu, J. Numerical simulation and case analysis of coal and gas outburst in the complex geological structure zone. *J. Anhui Univ. Sci. Technol. Nat. Sci.* **2016**, *365*, 5–10.
21. Li, H.; Lin, B.; Huang, Z.; Teng, F.; Yang, W.; Gao, Y.; Liu, T.; Wang, R. Stress and displacement evolution features of opening seam in mine cross cut based on different in-situ rock stress and orientations. *Coal Sci. Technol.* **2017**, *4510*, 88–95.
22. Zhao, B.; Wen, G.; Nian, J.; Ma, Q.; Fan, C.; Lv, X.; Deng, C. Numerical Simulation Study on the Multi-Physical Field Response to Underground Coal and Gas Outburst under High Geo-Stress Conditions. *Minerals* **2022**, *12*, 151. [[CrossRef](#)]
23. Hu, S.; Wang, E.; Kong, X. Damage and deformation control equation for gas-bearing coal and its numerical calculation method. *J. Nat. Gas. Sci. Eng.* **2015**, *25*, 166–179. [[CrossRef](#)]
24. Hu, S.; Li, X.; Wang, E. Experimental and Numerical Study on Scale Effects of Gas Emission from Coal Particles. *Transp. Porous. Media* **2016**, *1141*, 133–147. [[CrossRef](#)]
25. Hu, S.; Wang, E.; Li, X.; Bai, B. Effects of gas adsorption on mechanical properties and erosion mechanism of coal. *J. Nat. Gas. Sci. Eng.* **2016**, *30*, 531–538. [[CrossRef](#)]
26. Liu, A.; Liu, S. A fully-coupled water-vapor flow and rock deformation/damage model for shale and coal: Its application for mine stability evaluation. *Int. J. Rock. Mech. Min.* **2021**, *146*, 104880. [[CrossRef](#)]
27. Liu, Z.; Shu, L.; Huo, Z.; Fan, Y. Numerical Study on the Mechanism of Coal and Gas Outburst in the Coal Seam Thickening Area during Mining. *Energies* **2023**, *16*, 3288. [[CrossRef](#)]
28. Liu, X.; Zheng, Y.; Hao, Q.; Zhao, R.; Zhang, Z. Rock Damage Model Coupled Stress–Seepage and Its Application in Water Inrush from Faults in Coal Mines. *ACS Omega* **2022**, *7*, 13604–13614. [[CrossRef](#)]
29. Shu, L.; Yuan, L.; Li, Q.; Xue, W.; Zhu, N.; Li, Z. Response characteristics of gas pressure under simultaneous static and dynamic load: Implication for coal and gas outburst mechanism. *Int. J. Min. Sci. Technol.* **2023**, *33*, 155–171. [[CrossRef](#)]
30. Zhou, A.; Wang, K.; Wang, L.; Du, F.; Li, Z. Numerical simulation for propagation characteristics of shock wave and gas flow induced by outburst intensity. *Int. J. Min. Sci. Technol.* **2015**, *25*, 107–112. [[CrossRef](#)]
31. Kong, X.; Li, S.; Wang, E.; Wang, X.; Zhou, Y.; Ji, P.; Shuang, H.; Li, S.; Wei, Z. Experimental and numerical investigations on dynamic mechanical responses and failure process of gas-bearing coal under impact load. *Soil. Dyn. Earthquake. Eng.* **2021**, *142*, 106579. [[CrossRef](#)]
32. Wang, E.; Kong, X.; Hu, S.; Li, Z.; Liu, Q. Multi-scale Fractured Coal Gas–Solid Coupling Model and Its Applications in Engineering Projects. *Transport. Porous. Med.* **2018**, *121*, 703–724. [[CrossRef](#)]
33. Tao, Y.; Xu, J.; Cheng, M.; Li, S.; Peng, S. Theoretical analysis and experimental study on permeability of gas bearing coal. *Chin. J. Rock. Mech. Eng.* **2009**, *282*, 3363–3370.
34. Li, P.; Kong, X.; Lu, D. Mathematical modeling of flow in saturated porous media on account of fluid-structure coupling effect. *J. Hydrodyn.* **2003**, *184*, 419–426.
35. Liu, J.; Chen, Z.; Derek, E.; Qu, H.; Chen, D. Interactions of multiple processes during CBM extraction: A critical review. *Int. J. Coal. Geol.* **2011**, *87*, 175–189. [[CrossRef](#)]
36. Liu, J.; Elsworth, D. Evaluation of pore water pressure fluctuation around an advancing long wall panel. *Adv. Water. Res.* **1999**, *226*, 633–644. [[CrossRef](#)]

37. Wyss, M.; Brune, J.N. Seismic moment, stress, and source dimensions for earthquakes in the California-Nevada region. *J. Geophys. Res.* **1968**, *73*, 4681–4694. [[CrossRef](#)]
38. Hanks, T.C.; Kanamori, H. A moment magnitude scale. *J. Geophys. Res.* **1979**, *84*, 2348–2350. [[CrossRef](#)]
39. Gutenberg, B.; Richter, C.F. Seismicity of the earth *Geol. Soc. Am. Spec. Pap.* **1941**, *34*, 1–33. [[CrossRef](#)]
40. Wang, C.; Cheng, Y. Role of coal deformation energy in coal and gas outburst: A review. *Fuel* **2023**, *332*, 126019. [[CrossRef](#)]
41. Ma, Y.; Nie, B.; He, X.; Li, X.; Meng, J.; Song, D. Mechanism investigation on coal and gas outburst: An overview. *Int. J. Miner. Metall. Mater.* **2020**, *27*, 872–887. [[CrossRef](#)]
42. Zhang, G.; Wang, E. Risk identification for coal and gas outburst in underground coal mines: A critical review and future directions. *J. Nat. Gas. Sci. Eng.* **2023**, *118*, 205106. [[CrossRef](#)]

Disclaimer/Publisher’s Note: The statements, opinions and data contained in all publications are solely those of the individual author(s) and contributor(s) and not of MDPI and/or the editor(s). MDPI and/or the editor(s) disclaim responsibility for any injury to people or property resulting from any ideas, methods, instructions or products referred to in the content.